Journal of Colloid and Interface Science 628 (2022) 223–235

Contents lists available at ScienceDirect

Journal of Colloid and Interface Science

journal homepage: www.elsevier.com/locate/jcis

Spontaneously formed multiscale nano-domains in monophasic region of ternary solution

Mingbo Li, Lei Yi, Chao Sun *

Center for Combustion Energy, Key laboratory for Thermal Science and Power Engineering of Ministry of Education, Department of Energy and Power Engineering, Tsinghua University, Beijing 100084, China

GRAPHICAL ABSTRACT

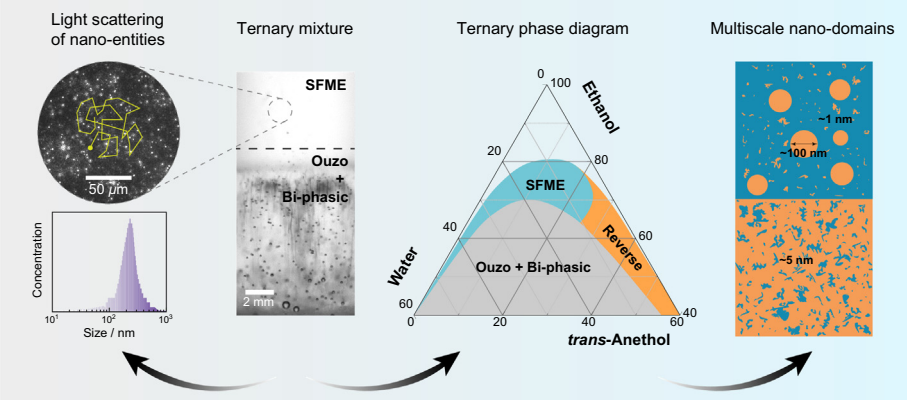

ARTICLE INFO

Article history:
Received 2 June 2022
Revised 23 July 2022
Accepted 25 July 2022
Available online 29 July 2022

Keywords:
Surfactant-free microemulsions
Mesoscale solubilization
Dynamic light scattering
Pre-Ouzo
Nanostructures

ABSTRACT

Hypothesis: Ternary mixtures, containing one hydrotrope and two immiscible fluids, both being soluble in the hydrotrope at any proportion, exhibit unexpected solubilization power and unusual mesoscopic properties, which are a subject of long-standing controversies for decades.
Experiments: This work investigates the entire monophasic region of ternary *trans*-anethol/ethanol/water system, where multiscale nanostructurings with correlation lengths exceeding dimensions of individual molecules are identified by dynamic light scattering. The physical properties of the ternary mixture are characterized, with revealing the compositional dependence of refractive index and dynamic viscosity.
Findings: In surfactant-free microemulsion (SFME) regime, the single phase consists of two distinct nanoscopic domains in equilibrium, one *trans*-anethol-rich aggregate at the molecular scale (∼1 nm) and one mesoscopic droplet at the mesoscale (∼100 nm). However, only a tiny fraction of the hydrophobic component *trans*-anethol (<∼0.025%) are initially incorporated in mesoscale structures, and the vast majority are molecularly dissolved or in the form of aggregates. The concentration of mesoscopic droplets increases sharply when shifting toward the miscibility gap, but their size exhibits a weak compositional dependence. The nanoscopic domains exhibit long-term physical stability, and the Ostwald ripening is still the primary mechanism governing such mesoscopic droplet aging, but with a rather low ripening rate.

* Corresponding author.
E-mail address: chaosun@tsinghua.edu.cn (C. Sun).

https://doi.org/10.1016/j.jcis.2022.07.152
0021-9797/

1. Introduction

Greek alcoholic beverage "Ouzo", Italy "Sambuca", French aperitif "Pernod" and Turkish beverage "Raki" are popular in daily life in Europe. These drinks are made by soaking plants in an ethanolic solution that contains some water-insoluble components [1,2]. Once supplemented with excessive water, these solutions turn into a milky white opaque colour with a large amount of micron-sized emulsion droplets nucleated spontaneously, a phenomenon known as the "Ouzo effect" [3]. More generally, the formation of Ouzo droplets is due to the spontaneous emulsification of two mutually immiscible components (usually oil and water) assisted by a third component (hydrotrope) in which both components are soluble (either completely or at least to a large degree) [4,5]. This special mixture system contains at least three components, and the "Ouzo effect" occurs in the miscibility gap of the ternary phase diagram. When the composition of the ternary mixture has not crossed the phase boundary (the water content is still low enough), the solution appears macroscopically homogeneous, stable and transparent, which is considered to be a monophasic solution by the naked eye. However, these monophasic systems are in fact structured and not molecular solutions as we have seen them. In particular, in the monophasic region close to the phase separation boundary, a significant light scattering signal not originating from individual molecules can be identified by means of wide-angle X-ray, small-angle scattering and neutron scattering [6,7].

If one of the components is amphiphilic molecule, more specifically surfactant, the formation of microemulsions usually occurs within a specific range of compositions. In addition to microemulsions, surfactants can form other types of nanostructures in solution, such as lyotropic liquid crystals and micelles. So far the standard theory of micellization has received widespread acceptance, which treats the solvent with monomers as a pseudo-phase in equilibrium with structured aggregates [8]. Unlike emulsion systems, classical microemulsions are thermodynamically stable and contain droplets typically ranging in diameter from 5 to 50 nm [9,10]. The role of the surfactant component is to act as a monomolecular film to separate the polar and non-polar liquids [10]. These well-defined structures thus depend significantly on the type and structure of surfactants, such as head-group area and surface charge regulation [11].

Recent studies from different groups have shown that similar structures with microemulsion nature have been found and characterized in liquid mixtures or ternary solutions even in the absence of surfactant [12–14,2,15]. The solutions usually contain hydrotropes, which are a class of amphiphilic molecules and usually short-chain alcohols, like n-propanol, ethanol, tertiary butyl alcohol (TBA), sodium cumenesulfonate, etc., that can increase dramatically the solubility of poorly soluble compounds in water [16,17]. They exhibit both surfactant-like and co-solvent properties, namely, dual actions in bulk solutions and interfaces [18]. But they differ from traditional surfactants because hydrotrope molecules have smaller non-polar tails and do not spontaneously assemble into distinct micelles in aqueous solutions [19]. Moreover, it is difficult to define hydrotrope unambiguously. They can be be neutral, as ethanol, or charged, and even are difficult to distinguish from co-solvents at the nanoscale and macroscopic thermodynamic level [20]. The Ouzo, consisting of water, ethanol and *trans*-anethol, is a typical ternary surfactant-free model system. The aforementioned presence of these surfactant-free structuring in the single-phase region of the ternary phase diagram has received extensive attention in recent years due to their ubiquity in various ternary mixtures. These yet-to-be-defined structures that differ from "standard" swollen micelles, have multiple terminology names, including detergentless microemulsions [4], "pre-Ouzo" [21], emphasizing its occurrence before enough water is added to induce the phase separation, surfactant-free microemulsions (SFME) [13,22–24], micellar-like structural fluctuations [25], mesoscale solubilization [12,26], being intermediate between molecular solubility and macroscopic phase separation, and ultraflexible microemulsions (UFMEs) [7]. These surfactant-free microemulsions, which occurs without application of external work, open up new perspectives on applications, such as drug delivery, catalysis, particle synthesis and detergency, especially where traditional surfactants are not suitable for addition [27–32,24].

Despite receiving extensive attention, qualitative microstructural studies of ternary systems have mainly focused on the existence and structure of aggregates. The mesoscale structures have been shown not to be unique to a certain ternary system, but to be ubiquitous in water/hydrotrope mixtures containing hydrophobic compounds, such as 1-octanol/ethanol/water, 2-octanol/1,5-pentanediol/water, oleic acid/n-propanol/water, octadecane/ethanol/water, Cyclohexane/TBA/water, and so on [6,17,33,15]. They are indeed physically existing entities with macroscopic lifetimes, rather than simple critical density fluctuations. Although the two are difficult to distinguish from length scale ($\sim$1 nm) and scattering spectra, concentration fluctuations are usually featureless changes in molecular concentration and relax by diffusion. Among them, the ternary system of octanol/ethanol/water has been extensively studied, and two distinct micelle-like aggregates or clusters with typical correction length of about $\sim$1 nm, one octanol-rich and one water-rich, were identified in the pre-Ouzo domain near the miscibility limit by scattering experiments and MD simulations [6,2]. As hydrotrope, the ethanol can be traced in both polar and nonpolar domains, and particularly have a strong affinity at the diffuse interface [13]. The hydration-entropy balance was introduced by Zemb et al. to explain the long-term stability of these nanoscopic structures [2]. The accumulation of ethanol molecules near the interface promotes the hydration interactions [34–37], which overcome the entropy and subsequently insert a net repulsive force between adjacent aggregates/clusters. These aggregates (occurring in water-rich domain of ternary systems) were shown to be only pronounced in the hydrotrope concentration range where molecular clustering and thermodynamic anomalies are observed in pristine binary hydrotrope/water solutions. In ternary solution of propylene oxide/TBA/water, however, the observed mesoscale structures were interpreted as the phenomenon of solubilization of oily impurities originally present in TBA and propylene oxide [33]. The inhomogeneities may exhibit abnormal curvature fluctuations in critical regions, resulting in the formation of a spongelike bicontinuous mesoscale structure. Moreover, the mesoscopic structures may behave as colloidal particles and thus can stabilize the bicontinuous phase formed in the oil/hydrotrope/water system near the critical point [38,26]. Still, the behavior of these inhomogeneities in the SFME or critical region is poorly understood and requires extensive research.

As a generic example of a large class of hydrophobe/hydrotrope/water ternary aqueous systems, the beverage Ouzo contain rather hydrophobic components like anisole, which is a poorly water-soluble aromatic ether, as a third component. In this work, we present a detailed and extensive experimental study focusing on the origin, nature, and occurrence of the multiscale microstructures coexisting in the ternary system of *trans*-anethole/ethanol/water. Two types of inhomogeneities, one at the molecular scale ($\sim$1 nm) and one at the mesoscopic scale ($\sim$100 nm), were identified in the monophasic region. Note that the molecular-scale and mesoscale inhomogeneities has previously been observed, but a quantitative analysis in terms of the correction of refractive index and viscosity has been lacking [21,39,15,40]. With precise refrac-

tive index and viscosity corrections, we were able to measure the correlation lengths of both simultaneously.

2. Experimental

2.1. Chemicals

Ultrapure water, with a conductivity of 18.2 MΩ · cm and a pH of 6.5 at 25°C, was received from a Milli-Q system (Merck, Germany). Ethanol (99.9%) was purchased from J&K Scientific (China). *trans*-Anethol with $M_w = 148.20$ (> 99%) was obtained from Sigma–Aldrich (Germany). All chemicals were used as received. The detailed information on the three components at 25°C are listed in Table 1. The density ρ, dynamic viscosity η and refractive index (RI) are given.

2.2. Experimental Setup

The sample preparation procedure is trivially simple and uniform: typically, the *trans*-anethol and ethanol were mixed first, then water was added in the desired proportion. All components were measured by volume with a laboratory scale, and a total volume of 50 mL of samples for each composition was prepared at room temperature (25°C). We define compositions based on the three volume fractions relative to ternary solutions: ϕ_a (*trans*-anethol), ϕ_e (ethanol) and ϕ_w (water), where $\phi_a + \phi_e + \phi_w = 100\%$. Hysteresis in experiments is observed, especially near the miscibility gap. So after mixing, a 10-min sonication in an ultrasonic cleaner (GS0304, 180 W, Granbo Technology, China) was applied to achieve adequate equilibration. At this point the ternary solution was stable and characterization was then performed within one hour. In the region far from the miscibility gap, the ternary solution is prepared at intervals of 5% by volume fraction. In the vicinity of the miscibility gap, the proportioning interval is narrowed to determine the transition from the single-phase region to the Ouzo region is determined as accurately as possible. All the ternary samples were prepared and stored in stoppered containers, to avoid changes in composition due to evaporation. The glass vials were firstly wiped with dust-free cloth moistened with ethanol to mechanically remove contaminants from the surface. Then they were sonicated in ethanol for 15 min, followed by successively washing with pure water, to remove any possible contaminants from the inner walls of the vials. We then blew the vials with nitrogen flow and dried them thoroughly in the oven for 1 h at 70°C. For each measurement, approximately 1 ml of sample is taken out with a glass dropper.

2.3. Dynamic Light Scattering (DLS)

The size of the nanostructures present in ternary solutions were characterized with dynamic light scattering (DLS) technique (ZEN3700 Zetasizer NanoZSE, Malvern Instruments) at 25°C. During measurements, a He-Ne laser with wavelength 632 nm as the light source was used, and the scattering angle was 173°. The refractive index of each ternary solution with a particular composition is corrected in advance (Measurement details are described below). The micron- and nano-entities in the size range of 0.4 nm∼10 μm hydrodynamic diameter can be identified. About 1 mL of the mixture was loaded into a glass cuvette with a light path of 10 mm and then the measurement was performed after equilibrating for 5 min. For each sample, two separate measurements were made, with each test repeated five times for better accuracy.

The basic theory is as follows. When a laser beam passes through a suspension containing particles or molecules undergoing Brownian motion (typically on the nanometer scale), there will be an attenuation or extinction in intensity [41]. The scattering light can fluctuate randomly in relation with Brownian motion. Smaller particles move faster, which in turn causes faster fluctuations in the intensity of scattering light. Specifically, the photocor correlator calculates the intensity auto-correlation function, an instrument output that can be further processed to obtain the size of nanostructures in a thermodynamically equilibrium system. Generally, quasi-random physical events can be described by correlation functions, which are mathematical structures designed to reflect the average time span over which signals remain correlated. In this study, we have no prior knowledge of the nanostructures that might exist in ternary solutions, substantially, the relaxation patterns. Here we use the double-exponential relaxation behavior as an example to introduce the calculation process. For a dilute solution, the intensity-related auto-correlation function of the double-exponential relaxation behavior can be given by the following equation

$$G^{(2)}(t) = [A_1 \exp(\frac{-t}{\tau_1}) + A_2 \exp(\frac{-t}{\tau_2})]^2 + 1 \quad (1)$$

where $A_{1,2}$ is the amplitude of the relaxation processes (an instrumental constant between 0∼1), t is the time delay of the photon correlations between signals, and, $\tau_{1,2}$ is the characteristic relaxation time. For the diffusive relaxation process, the relaxation time τ is related to the diffusion coefficient of the particles D_T, and follows $\tau_{1,2} = 1/D_T q^2$, where q is the norm of scattering vector (the difference in the wave number between incident and scattered light) [42,43]. Moreover, q can be related to the refractive index of the dispersion medium n, the scattering angle θ and the wavelength of the incident light λ with the equation $q = (4\pi n/\lambda)sin(\theta/2)$. Note that all calculations are performed using scattered light intensity, so the distributions of diffusion coefficient is weighted based on their scattering behavior. While DLS has been recognized as a standard technique widely used, one of the well-known drawbacks of DLS is the low peak resolution. Typically, DLS can only resolve particle populations that differ by at least a factor of three in size [44]. This means that these diffusion processes, either slow or fast, should be well separated and not disturb each other. Accordingly, the relaxation-time scales of the two modes should be significantly different (at least one decade in time) to distinguish different nanostructure populations in polydisperse samples.

Further, the hydrodynamic diameter of the non-interacting, spherical-assumed Brownian particles, D, can be calculated by the Stokes–Einstein equation [45]

$$D = \frac{k_B T}{3\pi\eta D_T}, \quad (2)$$

where k_B is the Boltzmann constant, T is the absolute temperature, and η is the dynamic viscosity of the dispersion medium. Under most circumstance of this study, the composition of the continuous

Table 1
Physical properties for three pure components at 25°C.

Component	Formula	ρ (kg/m^3)	η (mPa · s)	RI
Water	H_2O	997.05	0.879	1.3325
Ethanol	C_2H_6O	785.46	1.057	1.3601
trans-Anethol	$C_{10}H_{12}O$	988.3	2.340	1.5610

medium not only determines the formation of nanostructures, but also its physical parameters, such as viscosity and refractive index, are deeply involved in the calculation of hydrodynamic size. These parameters should be corrected prior to any DLS measurements. In this way, a link can be established between the macroscopic fluid physical properties and the microscopic composition of the solution.

In this study, the acquisition and analysis of the measurement data is performed in the "Malvern Zetasizer Nano software" equipped with the Malvern instrument. It controls the system during measurement and then processes the measurement data to ultimately obtain size results. Prior to characterization of a certain ternary mixture, information about the physical properties of this sample dispersant (dynamic viscosity and refractive index) under a certain temperature was added to the system as a new material. The raw correlation data (processed by the "Malvern Zetasizer Nano software") was extracted and then fitted using the two-term exponential method in Matlab. The characteristic relaxation time thus can be obtained.

2.4. Nanoparticle Tracking Analysis (NTA)

Nanoparticle tracking analysis (NTA) technology determines particle size by tracking and analyzing the trajectories described by individual particles in suspension. Moreover, it can image the particles 'directly' so that their number concentration can be easily obtained. Here a home-built NTA system, consisting of an optical darkfield microscope equipped with a high-speed camera, a laser and a glass sample cell, was applied. A finely focussed laser beam (wavelength of 520 nm) is refracted twice by a prism-edged optical flat and enters the sample micro-chamber with a height of 500 μm. The path of the laser in the sample is almost parallel to the glass-sample interface. Scattered light from particles residing in the beam path can be visualised with a long working distance objective ($\times$20 magnification) mounted on an inverted optical microscope (IX73, Olympus, Japan). The color image series can be captured by a high-sensitivity CCD camera (xiD, XIMEA, Germany) equipped onto the microscope at a framerate of 30 fps (resolution 1936$\times$1456). Typically five videos are recorded per sample, each video lasting 60 s long. The NTA measuring results were analyzed by ImageJ/Fiji [46], particularly the newly developed NanoTrackJ software [47], to obtain the information of particle concentration and size distribution. The temperature of the chamber was controlled at 25°C throughout the imaging process with a polyimide electrothermal film attached to the surface of the upper plate. After loading, the sample were thermally equilibrated for 5 min before recording was performed. For more details on the NTA system please refer to our previous work [48].

2.5. Measurements of viscosity, refractive index (RI) and turbidity

To extract accurately the size or correlation length of the nanostructures from DLS experiments, information on the refractive index and dynamic viscosity of the ternary mixture needs to be determined in advance. These parameters also reflect the macrophysical properties of the mixture.

The dynamic viscosity of each ternary mixture was directly measured using a rheometer (Discovery Hybrid Rheometer, TA Instruments, USA) in a double gap cylinder (Couette) configuration at 25°C. In particular, the viscosity-temperature characteristics of pure *trans*-anethole are shown in Figure S1.

Correspondingly, the refractive index was measured with an automatic refractometer (GR30, Shanghai Zhuoguang Instrument Technology, China) at 25°C for the ternary solutions. The values of viscosity for these solutions at other compositions were interpolated.

The turbidity of the ternary mixtures was measured using a turbidity meter (WZS-188, Shanghai INESA Scientific Instrument, China) at 25°C, which characterizes the ratio of scattered light intensity relative to transmitted light intensity. For each measurement, about 80 mL sample was needed. Turbidity information is used to obtain the phase separation line quantitatively. Turbidity measurements here are reported in nephelometric turbidity units (NTU). Since turbidity is obtained as a relative magnitude, for instance, 0 for pure water, calibration is performed using ultrapure water and a standard turbidity calibration solution (100 NTU, diluted from a standard sample of 400 NTU) prior to measurement. The measuring range of the instrument: 0$\sim$20 NTU, is selected, and the resolution is 0.01 NTU.

3. Results and discussion

3.1. Ternary phase diagram

trans-Anethol is insoluble with water, but both can be miscible with ethanol in any proportion. The three-component *trans*-anethol/ethanol/water mixtures outline a rich ternary phase diagram where distinct domains can be distinguished, as shown in Fig. 1. It was obtained at 25°C by multiple complementary methods, including visual observation, DLS technique and turbidimetry, for the ternary system over the whole range of volume fraction of the components (see Figure S2 in Supplementary Material for raw data). A set of phase transition points were obtained by titrating various *trans*-anethol/ethanol mixtures with water, and thus the miscibility gap of *trans*-anethol and water was established (the dashed line). A typical case, demonstrating the transition from a macroscopically transparent single-phase solution across the miscibility limit to a milky Ouzo emulsion, is shown in Figure S3. The miscibility-limit line (binodal) is the best fit of the experimental points obtained by sequentially adding water to a clear binary solution and then observing and measuring until the metastable Ouzo phenomenon pops up. Herein the determination of the transition points also takes into account the turbidity of the solution, which increases sharply with increasing water volume fraction (see Figure S4). Typically, the experimental results show that Ouzo

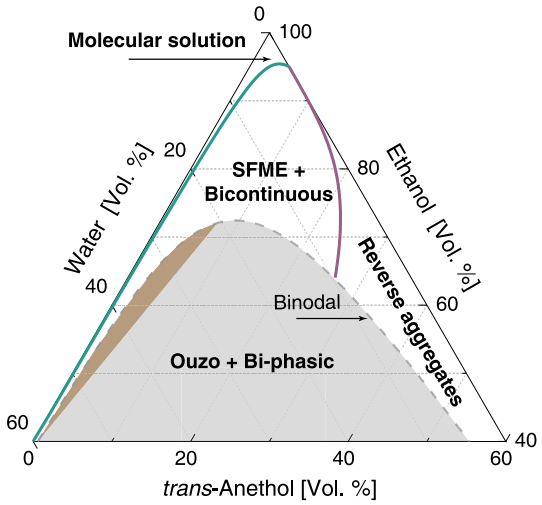

Fig. 1. Ternary phase diagram for the system of *trans*-anethole/ethanol/water in volume fractions at 25°C. The dashed line represents the miscibility limit between the pseudo-single phase domain and the multiphase domain (gray shaded area, including Ouzo and biphasic regions). The Ouzo zone (brown-filled) is roughly determined based on the data in previous work [49]. In the monophasic domain, three regimes are distinguished by solid lines. For clarity, only part of the complete phase diagram is shown.

effect occurs when the turbidity reaches about 10.5 NTU, at which point its corresponding composition can be determined. The Ouzo effect takes place in the portion of the phase diagram (brown-filled zone) in which *trans*-anethol is rather dilute ($\phi_a < 8\%$) as the solubility of *trans*-anethol in water is extremely low. Since the subject of our research is the monophasic region, we just roughly defined the Ouzo zone in the multiphasic region. The characteristic borders of this narrow zone can be found in previous work [49].

Note that, the monophasic domain, extending from water-rich part to *trans*-anethol-rich part, occupies only a small portion in this diagram. It corresponds to the samples which are macroscopically homogeneous and thermodynamically stable. This domain also represents the solubilization power of added ethanol to *trans*-anethol/water, leading to the formation of real molecular solutions or surfactant free microemulsions. This pseudo-single region, further, can be divided into three regimes, namely molecular solution, SFME + bicontinuous and reverse aggregates, depending on the microstructures present in the ternary mixtures. The regime of molecular solution only appears in a very narrow composition window where the ethanol content is very high ($\phi_e > 90\%$). It is represented by a spectrum with no particular scattering pattern in the DLS scattering signal. The regime where nanoscopic pseudophase can be observed directly by DLS typically is labeled as the SFME. The transition from the SFME regime to the reverse-aggregate regime is determined by DLS, marked by the disappearance of specific nanostructures (explained in detail in the following subsection), and occurs at around 25% *trans*-anethol content. The gap between these two regimes can be bridged by the bicontinuous regime, in which a phase inversion from a water-continuous solution to a *trans*-anethol-continuous solution occurs. In this study, bicontiguous regime was not separately distinguished from SFME region, but the two were merged together.

3.2. Refractive index and viscosity distribution

In order to extract the size of nanostructures under Brownian motion or correlation length of critical fluctuations from DLS measurements, the information on the shear viscosity and refractive index for each ternary solution need to be accurately corrected. Fig. 2 shows the measured data of refractive index and dynamic viscosity for the ternary mixture in the monophasic region. Both the phase diagrams are achieved by mapping of more than a hundred samples as well as spline interpolation of the points measured. We found that refractive index depends mainly on the *trans*-anethol volume fraction ϕ_a in the ternary mixture (see insert in Fig. 2(a) for more quantitative details), roughly, a linear relationship. In contrast, the increase in water volume fraction ϕ_w results in only a slight increase in RI. The RI of the ternary mixture, to some extent, can be roughly estimated according to the composition of the mixture without measurement.

Besides, the compositional dependence of viscosity shows a complex picture. Increasing the water or *trans*-anethol content both cause viscosity to increase. The measured viscosity as a function of the water fraction shows that their relationship is almost perfectly linear, as shown in the insert in Fig. 2(b). The maximum viscosity occurs in the region where the water fraction is approximately 45% and the *trans*-anethol content is relatively low. This can be related to the properties of binary mixtures of water/ethanol: the density and surface tension of water/ethanol mixtures have a monotonic behavior with ethanol fraction, while the viscosity does not [50,51]. These measurement results may reflect a generic nature of macrophysical properties for this class of ternary mixtures. Furthermore, one can also observe that there is no abrupt change in viscosity values even near the phase-separation boundary, indicating that the presence of nano-structures has a weak effect on viscosity.

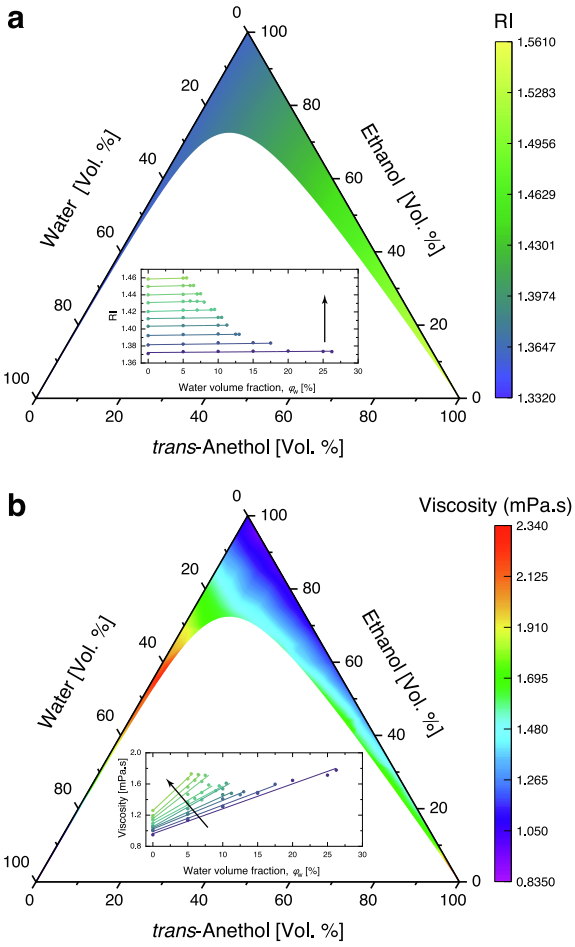

Fig. 2. Ternary phase diagram at 25°C in volume fraction for refractive index from refractometer measurements (a) and shear viscosity from rheometer measurement (b). The insert in each figure shows the effect of water content on RI and viscosity, respectively, for various *trans*-anethol fraction (5% ∼ 50%).

3.3. Compositional paths

In order to decouple, to some extent, the effects of individual components on the specific structures in various formulations, the co-solvency along three different compositional pathways within the monophasic region of the ternary phase diagram was studied using DLS. As shown in Fig. 3, the amounts of water, ethanol and *trans*-anethol were kept constant and equal to 5%, 75% and 5%, respectively.

As shown in Fig. 3(a), along Path I, the correlation functions progressively became more and more pronounced when moving close to the demixing line by increasing the amount of *trans*-anethol, ϕ_a, from 0 up to 50%. Correspondingly, the characteristic behavior of the intensity auto-correlation functions evolve from a double exponential ($<\sim 25\%$), namely, two different dynamic relaxation modes, to a single exponential ($\geqslant 25\%$), and the spatial coherence factor increases monotonously from 0.1 to nearly 0.9. As expected, the binary mixture of ethanol and water did not show any correlation. The characteristic time of the slow relaxation process τ falls within the range of $100 \sim 1000$ μs, and decreases with the increase of ϕ_a and finally vanishes at $\phi_a \sim 25\%$ (see figure on the right, left y-axis). The fast relaxation process persists within the studied range, and its characteristic time τ, on the scale of ~ 1 μs, increases slowly throughout the series. The τ presents a fairly wide distribution in the range from several microseconds to several hundreds of microseconds (at least two orders of magni-

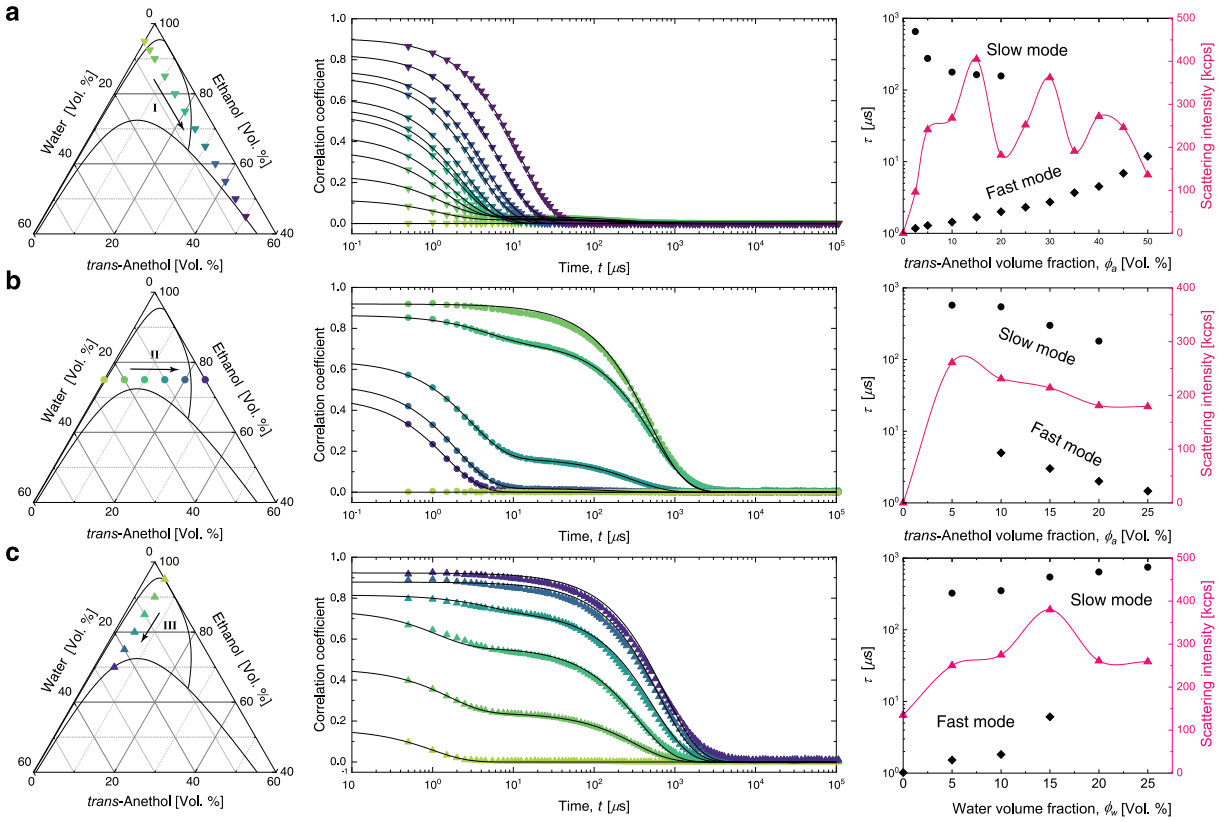

Fig. 3. Three different paths are identified with arrows and numbers: (a) I, keep water volume fraction constant at 5%, (b) II, keep ethanol volume fraction constant at 75%, and (c) III, keep *trans*-anethol volume fraction constant at 5%. The symbols indicate the various compositions of the ternary mixtures studied along these paths. The column in the middle shows DLS intensity auto-correlation functions for monophasic mixtures with the compositions shown on the ternary diagram on the left. The continuous lines are the best fit obtained according to Eq. (1). The right column shows the DLS characteristic relaxation time (left *y*-axis) and sacttering intensity (right *y*-axis) as a function of the volume fraction of *trans*-anethol or water.

tude). These two signal modes thus are easily distinguished on the DLS spectrum without overlapping interference. The scattering intensity first increases sharply, and then stays at high magnitude in an oscillating manner after passing the transition region (right *y*-axis). This path passes through three different sub-domains in succession. The increasing *trans*-anethol content shifts the functions to longer decay times (typically < 100 μs). Longer values correspond exactly to these ternary systems that are close to the phase separation, which in turn means an increase in the scattering intensity and sample turbidity.

Along Path II, these intensity auto-correlation functions were obtained by increasing the *trans*-anethol fraction with a fixed composition of 75% in ethanol, as shown in Fig. 3(b)). Apparently, the overall shape of the intensity auto-correlation functions differs prominently from that observed in Path I. Similarly, the liquid does not exhibit any diffusion relaxation behavior in the absence of *trans*-anethol. When tiny *trans*-anethol ($\phi_a = 5\%$) is added, the correlation function is a single exponential, suggesting an easily discernible length scale. Then a double exponential characteristic behavior appears as the *trans*-anethol/water volume fraction further increases. The correlations become less and less pronounced as the solution composition moves away from the miscibility gap. However, with the further reduction of water content, the auto-correlation function returns to a single exponential characteristic behavior, with only the fast relaxation mode retained. The characteristic times of both fast- and slow-relaxation processes decrease with increasing *trans*-anethol fraction. These series passes just above the critical point and facilitates the investigation of water/oil inversion. There is a huge cut gap in the DLS spectrum between the water-rich and *trans*-anethol-rich sides, which illustrates the transition between morphologies.

Along Path III, where the composition of *trans*-anethol is fixed at 5%, the intensity auto-correlation functions of these ternary samples gradually approaching the miscibility gap are obtained in Fig. 3(c). In the absence of water content, a single exponential relaxation behavior with characteristic time of $\sim$1 μs was observed. Then with increasing water fraction, a double exponential behavior with the coexistence of two relaxation processes, similar to that observed in Path II, emerges. In contrast, however, the characteristic time of both processes increases with the water fraction ϕ_w. When extremely close to the phase-separation border, the fast-relaxation process vanishes or becomes indistinguishable, leaving behind the slow relaxation process with a particularly high correlation coefficient (~ 0.9). Interestingly, the scattering intensity also decreases significantly with the disappearance of the fast-relaxation process. It can be seen that, the two-component analysis thus can provide important insights into the behaviour and microstructure for these ternary systems. These two coexisting characteristic relaxation behaviors, whose relaxation time differs by at least two orders of magnitude, are so different that they can be accurately captured using the double-exponential autocorrelation function. Basically, they can be considered as two domains of uncorrelated microstructures. The intensities of the two scattering patterns are also comparable, thus avoiding mutual cover-up.

3.4. Size of the multiscale coexisting nanostructures

The characteristic times corresponding to different dynamic modes essentially reflect the presence of nano-domains with well-defined size in the macroscopically homogeneous, monophasic region. With viscosity and RI corrections, in particular, it is possible to determine their dimensions using DLS. Herein the

influence of the shape of these nanoscale structures is ignored and the spherical geometry is uniformly assumed.

We start from the binary *trans*-anethol/ethanol solutions ($\phi_w = 0$) with various ϕ_a values. DLS data were collected for these mixtures with *trans*-anethol volume fraction increasing from 5% to 95%, as shown in Fig. 4. Unexpectedly, these systems are not homogeneous molecular solutions, but contain molecular-scale inhomogeneities with correlation lengths of order of ~ 1 nm. This scattering originates from the concentration fluctuations (clustering) occurring on the molecular scale. As the *trans*-anethol volume fraction ϕ_a increases, the distribution of the characteristic size expands and then remains constant when $\phi_a > 40\%$. However, the mean value of the characteristic size exhibits a non-monotonic dependence on ϕ_a with the maximum occurring at $\phi_a \sim 55\%$. Moreover, the inhomogeneities are only observed if *trans*-anethol volume fraction exceeds a threshold ($\sim$10%). A similar behavior was also observed in the aqueous mixtures, such as tert-butanol/water and 2-butoxyethanol/water, where the aggregates are though as a pre-micellar molecular arrangement. More specifically, even though hydrotropes do not spontaneously form stable micelles beyond a certain concentration like conventional surfactants, their aqueous solutions may exhibit dynamic, non-covalent molecular clustering [26]. They usually involve hydrogen bonds, and are short-ranged (order of $\sim$1 nm in size) and short-lived (a relaxation driven by reorientation of H-bonds). So far, we are not yet able to rationalize the appearence of these aggregates in this kind of ternary solution, and the non-monotonous dependence, and further research on this issue is needed.

We next investigate the nanoscale structures present in the monophasic region of the ternary phase diagram. Following the three pathways chosen before (see Fig. 3), we obtained the size of corresponding nanoscale structures, as shown in Fig. 5. It can be seen that the ternary solution contains multiscale nanostructures that span four orders of magnitude in equivalent sphere dimension. Clearly, there are at least two types of nanostructures coexisting here, corresponding to the aforementioned two relaxation modes in the scattering signal. Along Path I with a fixed water content ($\phi_w = 5\%$), the evolution of the size distribution of these nanostructures when increasing the volume fraction of *trans*-anethol ϕ_a is shown in Fig. 5(a). For the molecular-scale inhomogeneities (order of $\sim$1 nm in size), the well-defined monomodal peak first decays and then shifts to larger sizes with increasing ϕ_a. The mesoscale inhomogeneities (order of $\sim$100 nm in size), or mesoscopic droplets, however, exist only in solutions with low *trans*-anethol composition $\phi_a \leqslant 20\%$. With increasing ϕ_a this scattering structure gradually broadens in size but decays rapidly in intensity until it disappears. Although the origin of these spontaneously formed structures in SFME region, is not well understood, they have been widely reported in such ternary mixtures. These polydisperse weak-aggregates, designated as "ultra-flexible microemulsions" (UFMEs) [52], "clusters" [12] or "mesoscopic solubilization" [26], may be *trans*-anethol-rich or water-rich domains (reverse aggregates) [6]. For *trans*-anethol-rich aggregates, the *trans*-anethol molecules form the inner core of the body, which is swollen by the ethanol. But, most ethanol molecules are preferentially distributed on the interface of the aggregates, forming a hydrogen-bonded microemulsion-like hydrotrope-water shell [53,12]. These strong hydrogen bonds are formed by the hydroxyl groups of ethanol molecules and water molecules, which in turn form loose micelle-like networks. Part of the ethanol/water clusters surround the aggregates, protecting them from the water-rich environment. The aggregates thus are short-lived and have a fast dynamics with a relaxation driven by reorientation of hydrogen bonds [54].

Here one note that, the size obtained from the DLS measurement is the hydrodynamic diameter of a sphere whose average dif-

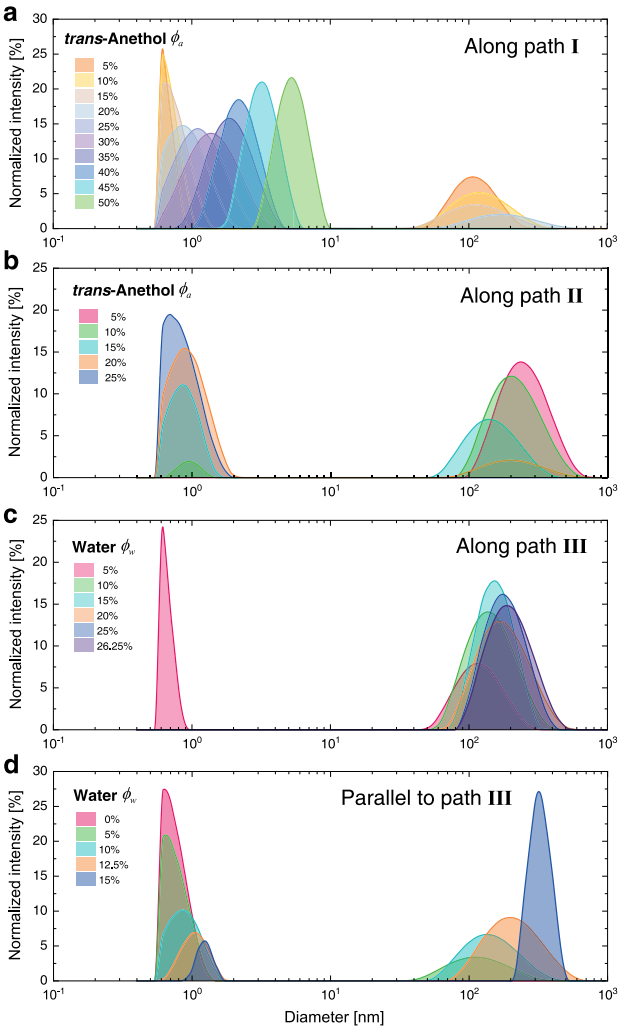

Fig. 5. Size distribution of the molecular-scale and mesoscale inhomogeneities observed in the monophasic domain of the ternary phase diagram. The samples shown in (a)$\sim$(c) correspond to the ternary mixtures on the three paths I, II, III shown in Fig. 3(a). The samples shown in (d), with a fixed *trans*-anethol volume fraction $\phi_a = 15\%$, falls on a path parallel to (c). For all the results, two types of nanostructures can be identified: *trans*-anethol-rich or water-rich aggregates at $\sim$1 nm scale (left peak) and mesoscopic droplets at $\sim$100 nm scale (right peak).

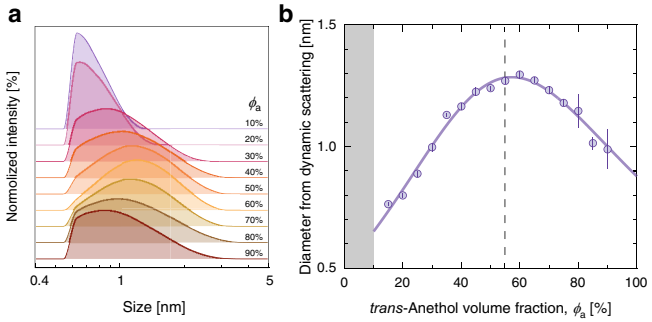

Fig. 4. (a) Size distribution and (b) mean correlation length of concentration fluctuations for binary *trans*-anethol/ethanol mixtures with varying volume fraction. The solid line presents the best fitting. The dashed line presents the peak. The shaded area marks that the mixture is pure molecular solution with no inhomogeneity detected.

fusion coefficient is the same as that of the object being measured. The rotational motion of the sphere is ignored. Given that the spontaneously formed nanostructures may not be perfectly spherical, especially those small-sized ones, the hydration and shape (conformation) could affect their behaviors. For these more general cases in which the entities are non-spherical or flexible, they could experience both translational diffusion and rotational diffusion. The rotational diffusion facilitates the randomization of the object orientation, which means that any structure that deviates from spherical will be treated as an "ellipsoid of revolution". The spherical approximation is a problem within the nature of DLS technology, and a direct consequence of this is that the diameter derived from the self-diffusion coefficient and the Stokes–Einstein relation (Eq. 2) may be smaller than the effective radius. Moreover, the translational diffusion coefficient also depends on a variety of other factors, such as the topology, adsorbing layer and chemical ordering of the nano-structure surface, which in turn cause the estimated size from DLS to be larger than the actual geometrical dimension. However, it is still possible to extract the dimension information for either spherical or anisotropic structures, for example, rod-like structures [55–57]. In this study, the classical Stokes–Einstein relationship is capable of obtaining the averaged dimension of these two kinds of nano-structure populations, respectively. Particularly, the bimodal mixture is composed of nano-structures differing sufficiently in size (two orders of magnitude). But a more specialized complementary characterization technique is needed to obtain their structural information.

In Path I, there are two types of *trans*-anethol-rich structuration, and we designate them as *trans*-anethol-rich aggregates (∼1 nm) and mesoscopic droplets (∼100 nm) depending on the symmetry (network or sphere), respectively. Note that, on this route towards the *trans*-anethol-rich corner, a phase inversion occurs, where the *trans*-anethol-rich aggregates are transformed into water-rich ones when the *trans*-anethol content is enough high ($\phi_a > 20\%$). The size or morphology of the water-rich aggregates is sensitive to the mixture components, and increases even to about 10 nm with increasing ϕ_a or decreasing ϕ_e. During the transition of the *trans*-anethol from the dispersed phase to the continuous phase, the water droplets are forced to clump together and become larger and larger. In a strong contrast, the features of *trans*-anethol-rich aggregates appear to exhibit a weak compositional dependence. This can also be inferred from the results of Path II, as shown in Fig. 5(b). Most of this path falls in the SFME domain. As the ϕ_a increases, a strong and sharp peak, centered around 1 nm, representing the *trans*-anethol-rich aggregates, develops. Furthermore, as expected, the transition of these solutions from an intermediate state, namely, mesoscale solubilization, to a state of molecular solubility occurs, resulting in the destabilization and disappearance of the mesoscopic droplets suspended therein. Fig. 5(c) illustrates the size distribution of the series of samples with compositions along Path III. Besides, another set of samples with compositions located on a path parallel to Path III is measured and summarized in Fig. 5 (d). Similarly, the content of *trans*-anethol is kept constant and equal to 15%. For these characteristic ternary mixtures, an increase in the volume fraction of water content induces the mixture to cross the miscibility gap from the SFME region until spontaneous emulsification occurs (Ouzo region). When the *trans*-anethol content is low (see Fig. 5(c)) the *trans*-anethol-rich aggregates are only present in the mixture with compositions far from the phase boundary. When $\phi_a = 15\%$, the structure of *trans*-anethol-rich aggregates gets weaker with increasing ϕ_w but can still be visible up to $\phi_w = 15\%$. In contrast, the mode of mesoscopic droplets become more pronounced, and the addition of water causes nucleation of more mesoscopic droplets within diameters between 50 and 500 nm from the excess *trans*-anethol still present.

We now link the mesoscopic droplets and the clustering present in the monophasic region to the micrometer-sized emulsion droplets in the Ouzo region, trying to answer how these nanostructures evolve into the microstructures, which has rarely been paid attention to in previous works [58,59,15,60]. In the stable Ouzo region of the ternary *trans*-anethol/ethanol/water system, the typical diameter of the dispersed emulsion droplets is ∼1 μm. Moreover, the droplet growth is dominated by Ostwald ripening, which has a saturation limit at a dropelet diameter of about ∼3 μm [49]. Herein two hypotheses can be proposed for the route of emulsion droplet formation after water addition: 1) the micrometer-sized Ouzo emulsion droplets are commonly formed by the coalescence of mesoscopic droplets; 2) the mesoscopic droplets grow continuously into Ouzo emulsion droplets under the action of molecular diffusion, in a manner akin to Ostwald ripening.

In SFME region, adding pure water to the homogeneous binary solution of *trans*-anethol/ethanol induces an abrupt drop of the solubility of *trans*-anethol in the water-rich continuous phase. A homogeneous nucleation at all points thus is expected, following the strong local concentration fluctuations of *trans*-anethol molecules. Ethanol, which is well miscible with water, acts as a carrier to uniformly distribute the *trans*-anethol molecules throughout the entire volume of the system, and then the *trans*-anethol begins to nucleate and aggregate. We also performed "visualizing" measurements on the ternary solutions using NTA technique, and representative snapshots for series of samples, which lie along a path parallel to Path III, are shown in Fig. 6(a). Concentration of *trans*-anethol was fixed at $\phi_a = 10\%$. Note that, in this view, only the mesoscopic droplets, namely Brownian diffusive droplets, are observed due to the optical resolution limitations of NTA (> 20 nm). With increasing ϕ_w (until near the phase-separation border), as expected, more mesoscopic droplets nucleate (the top row). A well-defined monomodal peak of the size-concentration distribution was observed, and it rises in a self-similar manner with ϕ_w (the bottom row). This indicates that the resulting mesoscopic droplets are relatively monodisperse. The peak size does not scale with increasing concentration of mesoscopic droplets but remains almost constant. Further, in Fig. 6(b), we show the total number concentration of the mesoscopic droplets as a function of the volume fraction of water ϕ_w. It is evident that, both water and oil content contribute to nucleation. For small content of the *trans*-anethol, droplet nucleation appears to reach a limit and maintain a slight increase as the composition approach the phase-separation boundary. For large ϕ_a, the concentration of nucleated mesoscopic droplets increases exponentially with the volume fraction of water, and the plateau is far from being reached even with extreme approaches to the boundary. Notably, there are still a lot of aggregates coexisting with the mesoscopic droplets in the ternary solutions.

We then roughly estimate the total volume of the mesoscopic droplets, for example, for a ternary solution with $\phi_a = 10\%$ and $\phi_w = 17.5\%$. In this case, the number concentration of mesoscopic droplets formed is as high as $\sim 2.5 \times 10^9$ droplet/mL, and a mean diameter of 200 nm is considered. After calculations (see Supplementary material for detailed calculation), we found that the *trans*-anethol in the form of mesoscopic droplets accounted for only ∼0.01% of the total added volume, suggesting that the *trans*-anethol phase prevailingly exists in the form of molecules and aggregates in SFME domain. Overall, only 0.001% to 0.025% of the *trans*-anethol phase exists as mesoscopic droplets in this ternary system (see Table S1). This also explains why mesoscopic droplets with a radius of ∼100 nm are "occasionally" observed and not identified in some other ternary systems, such as n-octanol/ethanol/water [7,52]. The size and presence of these meso-

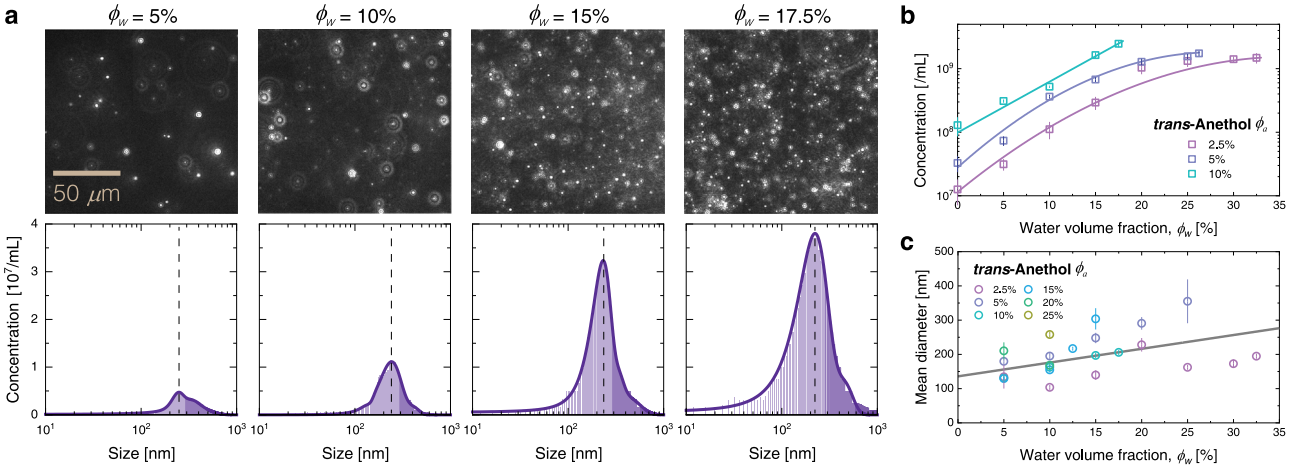

Fig. 6. (a) The NTA measuring results with increasing water volume fraction ϕ_w. The top row indicates a series of microscopic images from the NTA experiments capturing the presence and dynamics of mesoscopic droplets. The bottom row indicates the corresponding size distribution histogram for these cases. (b) Experimentally measured number density of mesoscopic droplets versus water volume fraction ϕ_w for various *trans*-anethol concentrations. (c) Mean diameter of the mesoscopic droplets nucleated in the SFME region, as a function of water volume fraction for various *trans*-anethol concentrations. Each data point in this figure is an average of five separate measurements, and the error bars denote the standard deviation over these measurements.

scopic droplets is sensitive to the chemical nature of the composition of the ternary system.

Even with such a drastic change in number concentration, the mean diameter of the mesoscopic droplets increases only slightly with ϕ_w, ranging from 100 to 300 nm, as shown in Fig. 6(c). In other words, there is no continuous evolution in the size of the mesoscopic droplets from ~100 nm to ~1 μm, but a sharp jump, even though the composition of the ternary mixtures is extremely close to the phase-separation boundary. Thereby, neither of the two assumptions listed above seem to hold. The Ouzo effect, presumably, occurs abruptly once the composition crosses the binodal, suggesting a local phase transition coupled strongly to the kinetic process [49]. On the phase-separation line, the mesoscale solubilization phenomenon begins to overlap with the Ouzo effect. But the connection between the two is not yet clear, and without doubt, this is a challenging task for researchers in this field.

In Fig. 7, we illustrate the representative snapshots of the continuous evolution of nano- and microstructures towards the water-rich corner or the *trans*-anethol-rich corner of the ternary phase diagram. Starting from the SFME region, with increasing *trans*-anethol content the mesoscopic droplets progressively vanish, while the *trans*-anethol-rich aggregates grow and interconnect randomly, forming a loose network and eventually a continuous phase. The situation is inversed, and numerous agglomerates of water molecules (reverse aggregates) are produced by extrusion and are swollen by ethanol. Note that, there is a bicontinuous domain between the SFME domain and the reverse-aggregate domain. It is a transition state where water and *trans*-anethol each form a sponge-like interwined network [37]. Under the case of interconnection, the water-rich or *trans*-anethol-rich regions may contain an additional structuring level, that overlaps the main existing aggregates in size. The overlap is probably a sign of structural changes, but it is difficult for DLS to distinguish these nanostructures from relaxation patterns. On the other hand, with increasing content of water, parts of the small clusters of *trans*-anethol combine to develop into mesoscopic droplets, and further micrometer-sized Ouzo emulsion droplets appear, coexisting with a small amount of aggregates. Note that mesoscopic droplets may also be present in Ouzo region, but have not been confirmed in this study.

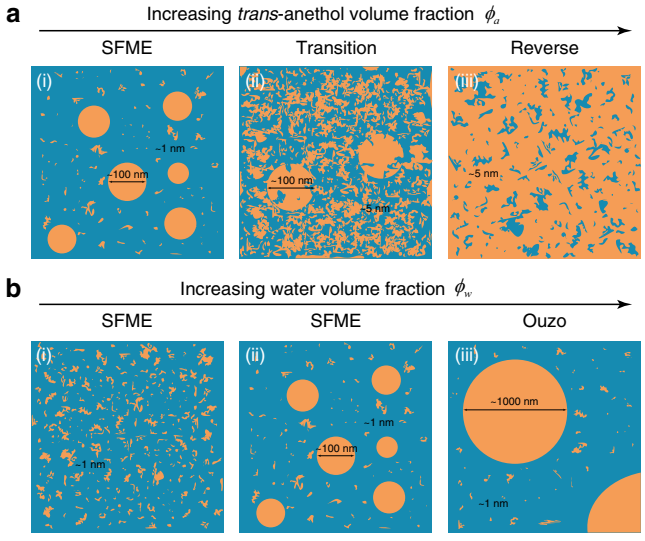

Fig. 7. Schematic representations of the evolution of nano- and microstructures towards the water-rich corner (a) or the *trans*-anethol-rich corner (b). The water-rich and *trans*-anethol-rich domains are marked in blue and orange, respectively.

3.5. Long-term stability

In this work, the stability and aging of the multiscale nanostructures was also studied in more detail. The Ouzo droplets have been shown to be remarkably stable, and can persist for days or even months [49]. Our long-term monitoring experiments show that these multiscale nanostructures in the ternary solutions with various compositions (see Fig. 8(a)) can also maintain long-term stability. The time dependence of three representative systems, i.e. with only mesoscopic droplets present (b), with only water-rich aggregates present (c), with both of *trans*-anethol-rich aggregates and mesoscopic droplets present (d~f), is compared. Herein one should note again that, the presence of peaks only for mesoscopic droplets in Fig. 8(b) does not imply the absence of aggregates in the solution system. It is because the content of aggregates is small that the scattering light intensity is too weak to be masked by that of the mesoscopic droplets (considering that the scattered light intensity is proportional to the sixth power of the diameter in the DLS measurement). The observations show that the size of

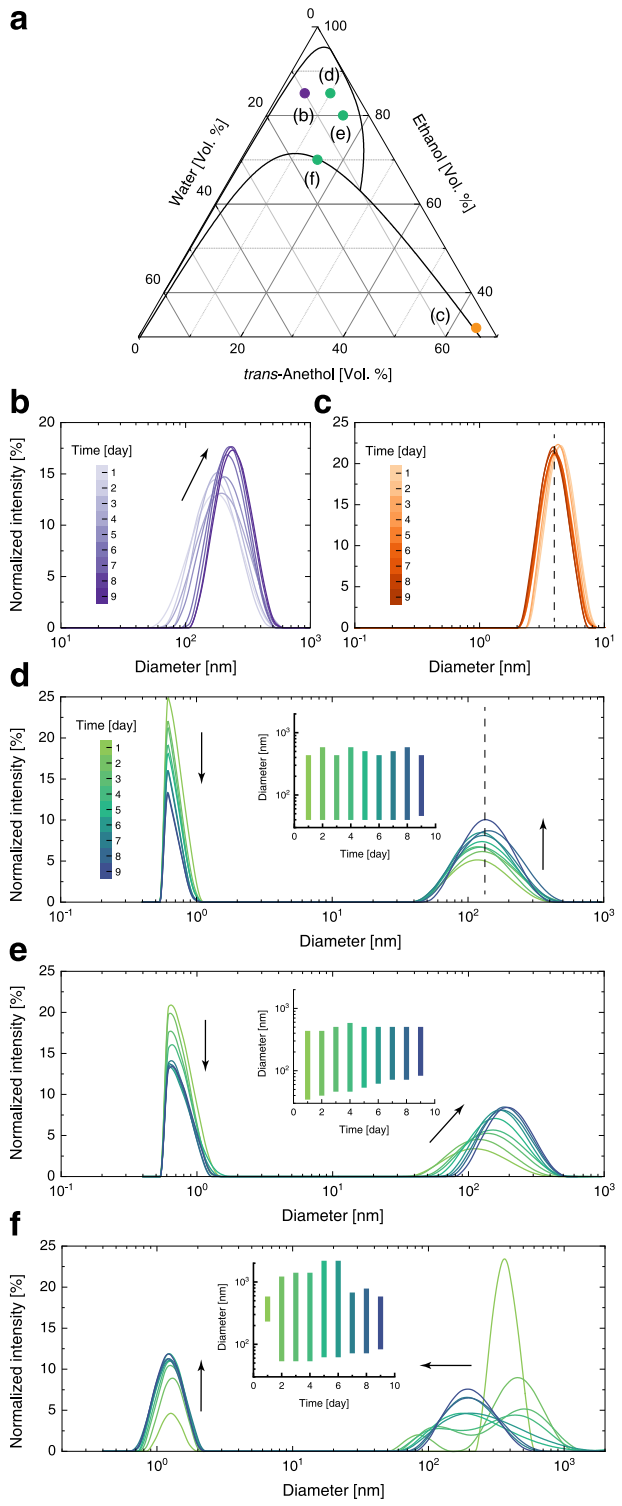

Fig. 8. Stability of the multiscale nanostructures. (a) Ternary phase diagram with the symbols indicating the different compositions studied. Long-term monitoring the measurements of ternary solutions with (b) only mesoscopic droplets present, (c) only reverse aggregates present, and (d∼f) aggregates and mesoscopic droplets coexisting.

mesoscopic droplets shifts to larger diameters over time, with a more concentrated distribution (see Fig. 8(b)). In contrast, the water-rich aggregates, present in the *trans*-anethol continuous phase, exhibit exceptional stability, with almost all size distribution curves overlapping (see Fig. 8(c)).

But do mesoscopic droplets in any case grow over time? In the ternary solutions, the aggregates dominate the bulk phase, and their number concentration is significantly higher than that of mesoscopic droplets. *trans*-Anethol molecules may be exchanged between aggregates and mesoscopic droplets via ethanol molecules as carriers, and after a sufficiently long time, a dynamic equilibrium is expected. Three distinct behaviors are observed when aggregates and mesoscopic droplets coexist, as shown in Fig. 8 (d∼f). The growth of these nano-domains is primarily governed by molecular diffusion. The scattered light intensity from detectable *trans*-anethol aggregates decays gradually, indicating a continuous consumption (see Fig. 8((d) and (e)). The loss or instability of the aggregates may be attributed to the destruction of the hydrogen-bonded shell of water and ethanol molecules. Correspondingly, the scattering light intensity from mesoscopic droplets is significantly enhanced. However, when the concentration of *trans*-anethol is low, the width of the size distribution hardly changes (see the insert of Fig. 8(d)), that is, the droplet size is almost constant over time. The enhancement of scattered light intensity is merely due to the nucleation of more mesoscopic droplets. In solutions with high *trans*-Anethol content, not only more mesoscopic droplets are generated but the droplets generally grew via molecular diffusion (see Fig. 8(e)). Moreover, the size distribution width of detectable mesoscopic droplets is significantly narrowed (see the insert of Fig. 8(e)), with droplets smaller than ∼90 nm in diameter disappearing on the last day of monitoring. The estimated Ostwald ripening rate is about 5.3×10^{-28} m^3/s, which is 5 orders of magnitude smaller than that of Ouzo droplets [49], indicating a extremely slow growth process.

Overall, the system with aggregates and mesoscopic droplets coexisting is practically stable, even with the exchange of components between the two nano-domains during aging. Then a question naturally arises here: are these nanostructures true equilibrium structures or kinetically trapped structures? These nanostructures appear to be non-equilibrium event if one considers the dependence on the mixing order of the three components [15]. However, the aggregates behave differently from mesoscopic droplets during aging, with their size remaining almost extremly constant. Once formed, these aggregates could be in thermodynamic equilibrium state, while mesoscopic droplets are likely kinetically trapped structures, but with a rather slow kinetics, presumably because of the high energy barrier. Note that thermodynamic solubility is indistinguishable under many cases from kinetically trapped state due to the quite slow kinetics. This issue is still controversial. The long-term stability may originate from the shielding effect that relies on the strong hydrogen bonds formed between ethanol and water molecules, and the preferential orientation of hydrotropes at the *trans*-anethol/water interface [61,62,18]. The shield physically isolates the hydrophobic core of mesoscopic droplets from the bulk solution, similar to surfactants thus reducing the effective surface tension. It may behaves like a rigid membrane that resists random deformation to make droplets smaller [8,63], or serves to stabilize the film of liquid between two approaching mesoscopic droplets. Furthermore, the negative-charge buildup on the droplet's surface, manifested as a high Zeta potential, may also stabilize the mesoscopic droplets and enhance the colloidal stability of the system [64]. For instance, our experimental results show that the mesoscopic droplets are negatively charged. Their Zeta potential is found to be generally greater than −10 mV (see Figure S5), which induces an electrostatic repulsion force high enough to resist coalescence.

However, when increasing the number concentration of mesoscopic droplets by the addition of water, we notice an opposite diffusion path: more aggregates were formed after several days with a decrease in the size of the mesoscopic droplets, as shown in Fig. 8

(f). This phenomenon reveals that, in SFME domain mesoscopic droplets with larger sizes, such as close to ~1 μm, are difficult to maintain long-term stability. The underlying mechanism causing the destabilization of large-sized mesoscopic droplets or the stabilization of specific-sized droplets, is still open so far. We infer, this is because the hydrogen-bonded shell at the droplet interface is not sufficient to bind such a bulky *trans*-anethol-rich core.

Furthermore, we obtain the evolution of the mean diameter of the mesoscopic droplets over the entire observation time. Fig. 9 presents the plots of the mean diameter as a function of time at different water concentrations and fixed *trans*-anethol concentration. At low *trans*-anethol concentration, the droplets were found to be stable and grow slightly with time (see Fig. 9(a)). Further we plot the mesoscopic droplets' volume as a function of time at various water volume fractions in Figure S6 (see Supplementary Material). As can be seen, all of the curves are linear within experimental error, suggesting that the central mechanism controlling aging in these solutions is Ostwald ripening [65,66]. Whereas at higher *trans*-anethol concentration, the trends strongly depend on the composition of the ternary solution, namely, the water/ethanol ratio (see Fig. 9(b)). After a long enough time, the droplet size returns to around 200 nm. For the cases with high water contents ($\phi_w \geqslant 12.5\%$), it is observed that the radius increases slightly for a short time and then decreases for a long time. Similar behavior was also observed in non-aqueous ternary mixture of octadecane/ethanol/ethylene glycol [15]. The former is likely caused by the Ostwald ripening, but with a higher ripening rate ($\sim 10^{-25}$ m^3/s), while the latter may imply a complex behavior. Combined with the experimental results in Fig. 8(f), the decrease in droplet size may originate from two factors: destabilization and sedimentation. The destabilization of mesoscopic droplets may promote the formation of more aggregates, as evidenced by the significantly enhanced scattered light intensity. The sedimentation may only occur with large-sized mesoscopic droplets, for example, larger than 1 μm in diameter, that settle to the bottom of the vessel against Brownian motion. The results also indicate that, the mesoscopic droplets larger than ~700 nm in diameter were no longer detectable after several days (see Fig. 8(f)). Here one should note that the size limit of the mesoscopic droplets (~700 nm) observed in the experiment is not consistent with what theory predicts. If we use the Peclet number to determine the buoyancy (gravity) threshold, as: $Pe = \pi\Delta\rho g D^4/24k_BT$, where $\Delta\rho$ is the density differences between the mesoscopic droplet and the medium liquid, g is the gravitational acceleration, k_B is the Boltzmann constant, and T is Kelvin temperature. If $Pe \leqslant 1$, the Brownian motion dominates and the mesoscopic droplets remain suspended freely. The calculated size limit according to this formula is around 1 μm, and thus more effort is needed to rationalize this gap. Indeed, the Ostwald ripening and even the final nanostructure size depend profoundly on the content of the dispersed *trans*-anethol-rich phase. Besides, interestingly, in the binary *trans*-anethol/ethanol solution without water addition, the nano-domains with diameters of around a few hundred nanometers are detected in the bulk after one day. It seems that, in such binary mixtures the quasi-equilibrium is distorted and the hydrophobes, which were initially dissolved in molecules, spontaneously aggregate into new large-sized inhomogeneities.

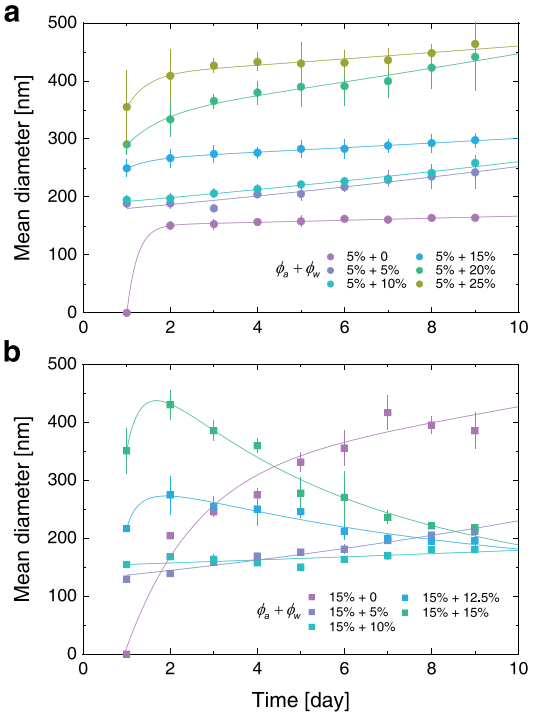

Fig. 9. Time evolution of the size of mesoscopic droplets formed at constant concentration of (a) *trans*-anethol $\phi_a = 5\%$ and (b) *trans*-Anethol $\phi_a = 15\%$ and varying concentrations of water ϕ_w. The solid lines represent the best fit.

4. Conclusions

Pre-Ouzo, SFME, UFME, micellar-like structural fluctuation or mesoscale solubilization, despite the various nomenclature, all refer to the same event occurring in the monophasic region of the ternary phase diagram for a broad class of ternary solutions "hydrophobe/hydrotrope/water", specifically, the water-rich side and near the phase-separation boundary. In similar ternary systems, it is a intermediate state between molecular solubility and macrophase separation, and even can coexist with both. This emerging phenomenology contains multiple mesoscopic-scale, hierarchically structured entities ranging from micelle-like aggregates/clusters to well-shaped mesoscopic particles/droplets. In this paper, we have investigated quantitatively these multiscale structuring that spontaneously forms in the macroscopically homogeneous, transparent moniphasic system of ternary solution *trans*-anethol/ethanol/water. Intuitively, using the same ternary system as a model, this work expands prior studies [3,49] by focusing our attention on the one-phase ternary solutions. The phase diagram characterized by volume fraction showed that the SFME regime occupies most of the single-phase region, while the molecular solution only appears in the ethanol-rich corner where the ethanol volume fraction exceeds about 90%.

The compositional dependence of ternary solution properties, including refractive index and dynamic viscosity, was systematically characterized. The results show that the solution RI only depends on the *trans*-anethol content over the entire composition range, while the dynamic viscosity exhibits a complex picture, i.e. increases with increasing *trans*-anethol content or water content (less than about 45%). The global maximum in viscosity occurs in the water-rich corners with a very low *trans*-anethol content. This may suggest a common picture of the compositional dependence of physical parameters for this class of ternary aqueous systems. Along with these two parameter corrections, the dynamic auto-correlation functions obtained from SFME region showed the presence of two distinct nanoscopic domains in equilibrium, one with *trans*-anethol-rich aggregates at the molecular scale (~1 nm) and one with mesoscopic droplets at the mesoscale (~100 nm). However, only a tiny fraction of the hydrophobic component *trans*-anethol (0.001~0.025%) are initially incorporated in mesoscale structures, and the vast majority are still molecularly dissolved or in the form of aggregates. The size of the mesoscopic

droplets, typically in the range of 100∼300 nm, has a weak dependence on the mixture composition, with no sign of evolution into micron-sized Ouzo droplets even very close to the phase-separation boundary. The concentration of mesoscopic droplets, however, is significantly dependent on the mixture composition, especially as further water is added, more mesoscopic droplets can be formed by consuming aggregates. The transition from the SFME regime to the reverse-aggregate regime is marked by the disappearance of structures in the vicinity of ∼100 nm, and occurs at around 25% *trans*-anethol content. In the *trans*-anethol-rich corner, the water-rich aggregates, with well-defined interface, are larger in size (∼5 nm) than the *trans*-anethol-rich ones, and increase upon increasing the water or *trans*-anethol content.

The nanoscopic domains in both SFME and reverse-aggregate regimes exhibit long-term physical stability with no apparent disappearance or coalescence. In the SFME region, the origin of the stability of these nano-domains may be twofold: well-shaped structuring of the individual itself, and colloidal stability between adjacent individuals (mesoscopic droplets). However, Ostwald ripening is still the primary mechanism governing mesoscopic droplet aging, but with a rather low ripening rate ($\sim 10^{-28}$ m^3/s). Due to the very slow kinetics, it is difficult to conclude whether they are thermodynamically equilibrium states or kinetically arrested events, which require further experimental and molecular dynamics simulation studies.

These nanoscale structures may to some extent determine the bulk properties of these complex solutions, such as solvation capacity or diffusion properties, which in turn affect their application performance. Although the obtained results in this work are for a given ternary system, these large-scale structures with similar characteristics, indeed are detected in some other aqueous mixtures and organic molecule solutions, thus implying a wide range of applications.

CRediT authorship contribution statement

Mingbo Li: Conceptualization, Methodology, Software, Validation, Formal analysis, Investigation, Writing original draft, Writing-review & editing, Visualization. **Lei Yi:** Methodology, Writing - Original Draft, Visualization, Validation. **Chao Sun:** Conceptualization, Supervision, Writing - Review & Editing, Funding acquisition, Project administration.

Declaration of Competing Interest

The authors declare that they have no known competing financial interests or personal relationships that could have appeared to influence the work reported in this paper.

Acknowledgments

We especially thank Detlef Lohse for his insights and fruitful discussions. This work was financially supported by the Natural Science Foundation of China under Grant Nos. 11988102 and 91852202, the China Postdoctoral Science Foundation under Grant No. 2020M680524, and Tencent Foundation through the XPLORER PRIZE.

Appendix A. Supplementary material

Supplementary data associated with this article can be found, in the online version, at https://doi.org/10.1016/j.jcis.2022.07.152.

References

[1] J. Marcus, M.L. Klossek, D. Touraud, W. Kunz, Nano-droplet formation in fragrance tinctures, Flavour Fragr. J. 28 (5) (2013) 294–299.
[2] T.N. Zemb, M. Klossek, T. Lopian, J. Marcus, S. Schöettl, D. Horinek, S.F. Prevost, D. Touraud, O. Diat, S. Marčelja, et al., How to explain microemulsions formed by solvent mixtures without conventional surfactants, Proc. Natl. Acad. Sci. 113 (16) (2016) 4260–4265.
[3] S.A. Vitale, J.L. Katz, Liquid droplet dispersions formed by homogeneous liquid-liquid nucleation:"the ouzo effect", Langmuir 19 (10) (2003) 4105–4110.
[4] G.D. Smith, C.E. Donelan, R.E. Barden, Oil-continuous microemulsions composed of hexane, water, and 2-propanol, J. Colloid Interface Sci. 60 (3) (1977) 488–496.
[5] A.R. Tehrani-Bagha, A. Viladot, K. Holmberg, L. Nordstierna, An ouzo emulsion of toluene in water characterized by nmr diffusometry and static multiple light scattering, Colloids Surf., A 494 (2016) 81–86.
[6] O. Diat, M.L. Klossek, D. Touraud, B. Deme, I. Grillo, W. Kunz, T. Zemb, Octanol-rich and water-rich domains in dynamic equilibrium in the pre-ouzo region of ternary systems containing a hydrotrope, Journal of applied Crystallography 46 (6) (2013) 1665–1669.
[7] S. Prevost, T. Lopian, M. Pleines, O. Diat, T. Zemb, Small-angle scattering and morphologies of ultra-flexible microemulsions, Journal of applied crystallography 49 (6) (2016) 2063–2072.
[8] J.N. Israelachvili, Intermolecular and surface forces, Academic press, 2011.
[9] P. Winsor, Hydrotropy, solubilisation and related emulsification processes, Trans. Faraday Soc. 44 (1948) 376–398.
[10] H.-F. Eicke, Surfactants in nonpolar solvents, Micelles (1980) 85–145.
[11] C. Tanford, Micelle shape and size, The Journal of Physical Chemistry 76 (21) (1972) 3020–3024.
[12] D. Subramanian, C.T. Boughter, J.B. Klauda, B. Hammouda, M.A. Anisimov, Mesoscale inhomogeneities in aqueous solutions of small amphiphilic molecules, Faraday discussions 167 (2013) 217–238.
[13] S. Schoettl, J. Marcus, O. Diat, D. Touraud, W. Kunz, T. Zemb, D. Horinek, Emergence of surfactant-free micelles from ternary solutions, Chemical Science 5 (8) (2014) 2949–2954.
[14] W. Hou, J. Xu, Surfactant-free microemulsions, Current Opinion in Colloid & Interface Science 25 (2016) 67–74.
[15] D. Rak, M. Sedlak, On the mesoscale solubility in liquid solutions and mixtures, J. Phys. Chem. B 123 (6) (2018) 1365–1374.
[16] T.K. Hodgdon, E.W. Kaler, Hydrotropic solutions, Current opinion in colloid & interface science 12 (3) (2007) 121–128.
[17] J. Xu, A. Yin, J. Zhao, D. Li, W. Hou, Surfactant-free microemulsion composed of oleic acid, n-propanol, and h2o, J. Phys. Chem. B 117 (1) (2013) 450–456.
[18] A.A. Novikov, A.P. Semenov, A.A. Kuchierskaya, D.S. Kopitsyn, V.A. Vinokurov, M.A. Anisimov, Generic nature of interfacial phenomena in solutions of nonionic hydrotropes, Langmuir 35 (41) (2019) 13480–13487.
[19] J. Eastoe, M.H. Hatzopoulos, P.J. Dowding, Action of hydrotropes and alkyl-hydrotropes, Soft Matter 7 (13) (2011) 5917–5925.
[20] W. Kunz, K. Holmberg, T. Zemb, Hydrotropes, Current Opinion in Colloid & Interface Science 22 (2016) 99–107.
[21] M.L. Klossek, D. Touraud, T. Zemb, W. Kunz, Structure and solubility in surfactant-free microemulsions, ChemPhysChem 13 (18) (2012) 4116–4119.
[22] J. Xu, J. Song, H. Deng, W. Hou, Surfactant-free microemulsions of 1-butyl-3-methylimidazolium hexafluorophosphate, diethylammonium formate, and water, Langmuir 34 (26) (2018) 7776–7783.
[23] X. Yan, P. Alcouffe, G. Sudre, L. David, J. Bernard, F. Ganachaud, Modular construction of single-component polymer nanocapsules through a one-step surfactant-free microemulsion templated synthesis, Chem. Commun. 53 (8) (2017) 1401–1404.
[24] X. Yan, J. Bernard, F. Ganachaud, Nanoprecipitation as a simple and straightforward process to create complex polymeric colloidal morphologies, Adv. Colloid Interface Sci. 294 (2021) 102474.
[25] A.A. Novikov, A.P. Semenov, V. Monje-Galvan, V.N. Kuryakov, J.B. Klauda, M.A. Anisimov, Dual action of hydrotropes at the water/oil interface, The Journal of Physical Chemistry C 121 (30) (2017) 16423–16431.
[26] A.E. Robertson, D.H. Phan, J.E. Macaluso, V.N. Kuryakov, E.V. Jouravleva, C.E. Bertrand, I.K. Yudin, M.A. Anisimov, Mesoscale solubilization and critical phenomena in binary and quasi-binary solutions of hydrotropes, Fluid Phase Equilib. 407 (2016) 243–254.
[27] K. Bouchemal, S. Briançon, E. Perrier, H. Fessi, Nano-emulsion formulation using spontaneous emulsification: solvent, oil and surfactant optimisation, International journal of pharmaceutics 280 (1–2) (2004) 241–251.
[28] V.K. Srivastava, G. Kini, D. Rout, Detergency in spontaneously formed emulsions, Journal of colloid and interface science 304 (1) (2006) 214–221.
[29] N. Anton, J.-P. Benoit, P. Saulnier, Design and production of nanoparticles formulated from nano-emulsion templates–a review, Journal of controlled release 128 (3) (2008) 185–199.
[30] N. Anton, T.F. Vandamme, The universality of low-energy nano-emulsification, International journal of pharmaceutics 377 (1–2) (2009) 142–147.
[31] J. Xu, H. Deng, J. Song, J. Zhao, L. Zhang, W. Hou, Synthesis of hierarchical flower-like mg2al-cl layered double hydroxide in a surfactant-free reverse microemulsion, Journal of colloid and interface science 505 (2017) 816–823.
[32] D. Liu, Z. Huang, Y. Suo, P. Zhu, J. Tan, H. Lu, Co2-responsive surfactant-free microemulsion, Langmuir 34 (30) (2018) 8910–8916.

[33] D. Subramanian, J.B. Klauda, P.J. Collings, M.A. Anisimov, Mesoscale phenomena in ternary solutions of tertiary butyl alcohol, water, and propylene oxide, J. Phys. Chem. B 118 (22) (2014) 5994–6006.
[34] S. Marcelja, Hydration in electrical double layers, Nature 385 (6618) (1997) 689–690.
[35] S. Marčelja, Hydration forces near charged interfaces in terms of effective ion potentials, Current opinion in colloid & interface science 16 (6) (2011) 579–583.
[36] S.H. Donaldson Jr, A. Røyne, K. Kristiansen, M.V. Rapp, S. Das, M.A. Gebbie, D.W. Lee, P. Stock, M. Valtiner, J. Israelachvili, Developing a general interaction potential for hydrophobic and hydrophilic interactions, Langmuir 31 (7) (2015) 2051–2064.
[37] T. Lopian, S. Schottl, S. Prevost, S. Pellet-Rostaing, D. Horinek, W. Kunz, T. Zemb, Morphologies observed in ultraflexible microemulsions with and without the presence of a strong acid, ACS central science 2 (7) (2016) 467–475.
[38] E.M. Herzig, K. White, A.B. Schofield, W.C. Poon, P.S. Clegg, Bicontinuous emulsions stabilized solely by colloidal particles, Nature materials 6 (12) (2007) 966–971.
[39] A. Lucia, P.G. Argudo, E. Guzmán, R.G. Rubio, F. Ortega, Formation of surfactant free microemulsions in the ternary system water/eugenol/ethanol, Colloids Surf., A 521 (2017) 133–140.
[40] Y. Zhang, X. Chen, X. Liu, Temperature-induced reversible-phase transition in a surfactant-free microemulsion, Langmuir 35 (44) (2019) 14358–14363.
[41] I. ISO13321, Methods for determination of particle size distribution part 8: Photon correlation spectroscopy, International Organisation for Standardisation (ISO) (1996).
[42] B. Chu, Laser light scattering: basic principles and practice, Courier Corporation, 2007.
[43] D. Subramanian, D.A. Ivanov, I.K. Yudin, M.A. Anisimov, J.V. Sengers, Mesoscale inhomogeneities in aqueous solutions of 3-methylpyridine and tertiary butyl alcohol, Journal of Chemical & Engineering Data 56 (4) (2011) 1238–1248.
[44] V. Filipe, A. Hawe, W. Jiskoot, Critical evaluation of nanoparticle tracking analysis (nta) by nanosight for the measurement of nanoparticles and protein aggregates, Pharmaceutical research 27 (5) (2010) 796–810.
[45] B.J. Berne, R. Pecora, Dynamic light scattering: with applications to chemistry, biology, and physics, Courier Corporation (2000).
[46] J. Schindelin, I. Arganda-Carreras, E. Frise, V. Kaynig, M. Longair, T. Pietzsch, S. Preibisch, C. Rueden, S. Saalfeld, B. Schmid, et al., Fiji: an open-source platform for biological-image analysis, Nature methods 9 (7) (2012) 676–682, https://doi.org/10.1038/nmeth.2019.
[47] T. Wagner, H.-G. Lipinski, M. Wiemann, Dark field nanoparticle tracking analysis for size characterization of plasmonic and non-plasmonic particles, Journal of nanoparticle research 16 (5) (2014) 2419, https://doi.org/10.1007/s11051-014-2419-x.
[48] M. Li, X. Ma, J. Eisener, P. Pfeiffer, C.-D. Ohl, C. Sun, How bulk nanobubbles are stable over a wide range of temperatures, J. Colloid Interface Sci. 596 (2021) 184–198.
[49] N.L. Sitnikova, R. Sprik, G. Wegdam, E. Eiser, Spontaneously formed trans-anethol/water/alcohol emulsions: mechanism of formation and stability, Langmuir 21 (16) (2005) 7083–7089.
[50] B. González, N. Calvar, E. Gómez, Á. Domínguez, Density, dynamic viscosity, and derived properties of binary mixtures of methanol or ethanol with water, ethyl acetate, and methyl acetate at t=(293.15, 298.15, and 303.15) k, J. Chem. Thermodyn. 39 (12) (2007) 1578–1588.
[51] G. Rage, O. Atasi, M. Wilhelmus, J.F. Hernández-Sánchez, B. Haut, B. Scheid, D. Legendre, R. Zenit, Bubbles determine the amount of alcohol in mezcal, Scientific reports 10 (1) (2020) 1–16.
[52] S. Prévost, S. Krickl, S. Marcelja, W. Kunz, T. Zemb, I. Grillo, Spontaneous ouzo emulsions coexist with pre-ouzo ultraflexible microemulsions, Langmuir 37 (13) (2021) 3817–3827.
[53] Z. Li, H. Cheng, J. Li, J. Hao, L. Zhang, B. Hammouda, C.C. Han, Large-scale structures in tetrahydrofuran–water mixture with a trace amount of antioxidant butylhydroxytoluene (bht), J. Phys. Chem. B 115 (24) (2011) 7887–7895.
[54] E.D. Sloan Jr, C.A. Koh, Clathrate hydrates of natural gases, CRC Press, 2007.
[55] J. Phalakornkul, A. Gast, R. Pecora, Rotational and translational dynamics of rodlike polymers: a combined transient electric birefringence and dynamic light scattering study, Macromolecules 32 (9) (1999) 3122–3135.
[56] D. Farrell, C.L. Dennis, J. Lim, S.A. Majetich, Optical and electron microscopy studies of schiller layer formation and structure, Journal of colloid and interface science 331 (2) (2009) 394–400.
[57] J. Lim, S.P. Yeap, H.X. Che, S.C. Low, Characterization of magnetic nanoparticle by dynamic light scattering, Nanoscale research letters 8 (1) (2013) 1–14.
[58] D. Subramanian, M.A. Anisimov, Phase behavior and mesoscale solubilization in aqueous solutions of hydrotropes, Fluid Phase Equilib. 362 (2014) 170–176.
[59] S. Schöttl, D. Horinek, Aggregation in detergent-free ternary mixtures with microemulsion-like properties, Current Opinion in Colloid & Interface Science 22 (2016) 8–13.
[60] S. Schöttl, T. Lopian, S. Prévost, D. Touraud, I. Grillo, O. Diat, T. Zemb, D. Horinek, Combined molecular dynamics (md) and small angle scattering (sas) analysis of organization on a nanometer-scale in ternary solvent solutions containing a hydrotrope, Journal of colloid and interface science 540 (2019) 623–633.
[61] A. Fiore, V. Venkateshwaran, S. Garde, Trimethylamine n-oxide (tmao) and tert-butyl alcohol (tba) at hydrophobic interfaces: Insights from molecular dynamics simulations, Langmuir 29 (25) (2013) 8017–8024.
[62] A.A. Kuchierskaya, A.P. Semenov, A.R. Sayfutdinova, D.S. Kopitsyn, V.A. Vinokurov, M.A. Anisimov, A.A. Novikov, Interfacial tension and phase properties of water–hydrotrope–oil solutions: water–2-butoxyethanol–toluene, J. Mol. Liq. 344 (2021) 117683.
[63] S.A. Safran, Statistical thermodynamics of surfaces, interfaces, and membranes, CRC Press, 2018.
[64] K. Marinova, R. Alargova, N. Denkov, O. Velev, D. Petsev, I. Ivanov, R. Borwankar, Charging of oil- water interfaces due to spontaneous adsorption of hydroxyl ions, Langmuir 12 (8) (1996) 2045–2051.
[65] I.M. Lifshitz, V.V. Slyozov, The kinetics of precipitation from supersaturated solid solutions, Journal of physics and chemistry of solids 19 (1–2) (1961) 35–50.
[66] P. Taylor, Ostwald ripening in emulsions, Advances in colloid and interface science 75 (2) (1998) 107–163.